ACS APPLIED MATERIALS & INTERFACES

Research Article

www.acsami.org

Ionic Liquid Assisted Chemical Strategy to TiO_2 Hollow Nanocube Assemblies with Surface-Fluorination and Nitridation and High Energy Crystal Facet Exposure for Enhanced Photocatalysis

Shengli Yu,[†] Baocang Liu,[†,‡] Qin Wang,[†] Yuxi Gao,[†] Ying Shi,[†] Xue Feng,[†] Xiaoting An,[†] Lixia Liu,[†] and Jun Zhang*[,†,‡]

[†]College of Chemistry and Chemical Engineering & Inner Mongolia Key Lab of Nanoscience and Nanotechnology, Inner Mongolia University, Hohhot 010021, People's Republic of China

[‡]College of Life Science, Inner Mongolia University, Hohhot 010021, People's Republic of China

Supporting Information

ABSTRACT: Realization of anionic nonmetal doping and high energy crystal facet exposure in TiO_2 photocatalysts has been proven to be an effective approach for significantly improving their photocatalytic performance. A facile strategy of ionic liquid assisted etching chemistry by simply hydrothermally etching hollow TiO_2 spheres composed of TiO_2 nanoparticles with an ionic liquid of 1-butyl-3-methylimidazolium tetrafluoroborate without any other additives is developed to create highly active anatase TiO_2 nanocubes and TiO_2 nanocube assemblies. With this one-pot ionic liquid assisted etching process, the surface-fluorination and nitridation and high energy {001} crystal facets exposure can be readily realized simultaneously. Compared with the benchmark materials of P25 and TiO_2 nanostructures with other hierarchical architectures of hollow spheres, flaky spheres, and spindles synthesized by hydrothermally etching hollow TiO_2 spheres with nonionic liquid of NH_4F, the TiO_2 nanocubes and TiO_2 nanocube assemblies used as efficient photocatalysts show super high photocatalytic activity for degradation of methylene blue, methyl orange, and rhodamine B, due to their surface-fluorination and nitridation and high energy crystal facet exposure. The ionic liquid assisted etching chemistry is facile and robust and may be a general strategy for synthesizing other metal oxides with high energy crystal facets and surface doping for improving photocatalytic activity.

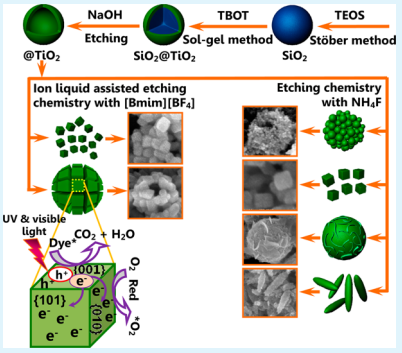

KEYWORDS: *ionic liquid, fluorination, nitridation, TiO_2 nanocube, high energy crystal facets*

1. INTRODUCTION

Titanium dioxide (TiO_2), a widely investigated semiconductor, can be utilized in environmental and energy issues,[1−4] particularly in photocatalysis,[5−7] due to its good photocatalytic activity, high chemical and thermal stability, nontoxicity, and excellent degradation capacity. However, its practical application has been impeded by its low utilization efficiency of solar energy and low quantum yield due to its wide band gap and high recombination rate of photogenerated charge carriers.[4] So, improvement in the catalytic activity of TiO_2 nanocrystals has been researched in both theoretical and experimental aspects in enormous works.[3−7] It is widely accepted that the crystal phase, doping, crystallinity, size, morphology, specific surface area, and architecture are all crucial factors that affect the catalytic activity of TiO_2 photocatalysts.[8] Doping with an anionic nonmetal atom such as fluorine (F),[9,10] nitrogen (N),[5] sulfur (S),[11] carbon (C),[12] and boron (B)[13] is demonstrated to be a useful strategy to enhance the photocatalytic activity of TiO_2 photocatalysts since the doped impurities can create localized states in the band gap of TiO_2 and induce visible light absorption.[14−16] Besides, the exposure of high energy crystal facets of TiO_2 photocatalysts through different synthetic strategies has been proven to be another effective approach developed lately to significantly improve its catalytic performance.[17] It is revealed that the crystal growth usually results in the reduction of highly active facets so as to minimize the surface energy. For anatase TiO_2, the theoretical calculation revealed that the {001} facets with a high surface energy are more reactive than the thermodynamically stable {101} facets.[6,8,18] To demonstrate this, the synthesis of various TiO_2 nanostructures with high energy surfaces exposed has attracted great interest and exploration.[7,19−28] Yang and co-workers conducted the pioneer works on the realization of high photocatalytic activity in anatase TiO_2 superstructures with an exposed high percentage of {001} facets around 47%.[7,20] It is indicated that the mean surface energies of anatase TiO_2 are the 0.44 J/m^2 of {101} facets, 0.53 J/m^2 of {100} facets, 0.90 J/m^2 of {001} facets, and 1.09 J/m^2 of {110} facets.[8] Because of the instability of the high energy crystal facets, it is a great challenge

Received: March 20, 2014
Accepted: June 1, 2014
Published: June 2, 2014

Scheme 1. Synthesis of TiO_2 Photocatalysts with Various Morphologies Synthesized by Hydrothermally Etching @TiO_2 with [Bmim][BF_4] and NH_4F under Different Reaction Conditions

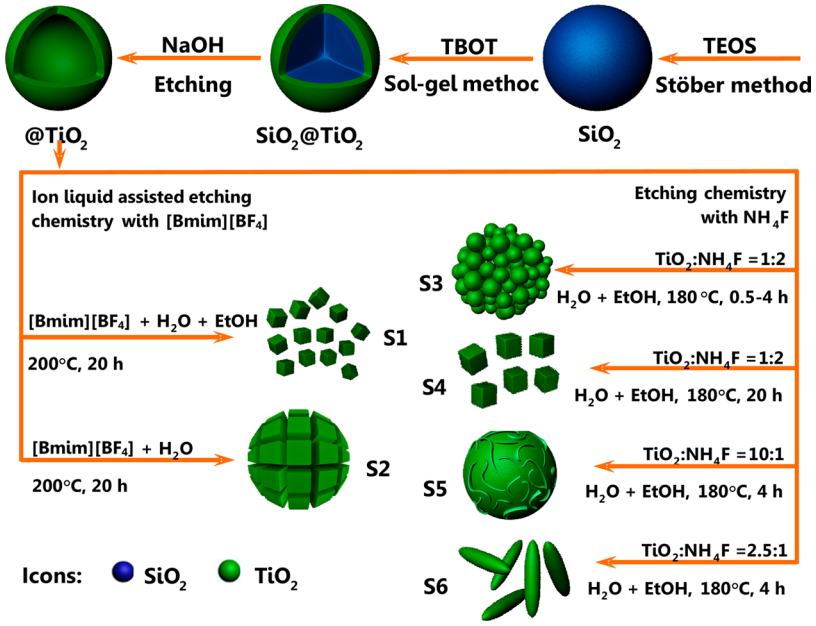

to synthesize anatase TiO_2 nanostructures with exposed high energy crystal facets corresponding to high catalytic activity.

The previously reported methods for creating TiO_2 nanostructures with high catalytic activity facets, such as {001} and {100}, always involve the use of extremely corrosive and toxic hydrofluoric acid (HF) or ammonium fluoride (NH_4F),[7,9,10,16,29−36] which imposes the restrictions on the practical application of TiO_2 photocatalysts.[64] Moreover, TiO_2 photocatalysts with the exposed high energy {001} crystal facets, normally in form of nanocubes,[37−39] are liable to deactivate and lack of chemical durability during the catalytic process due to its extremely active nature. Therefore, the strategy to generate TiO_2 nanocube assemblies possessing the improved catalytic activity and enhanced chemical durability is crucially important for such nanocube TiO_2 photocatalysts to be used further in practice. It is highly desirable to achieve such nanocube TiO_2 photocatalysts with highly reactive {001} facets exposed in a chemistry way instead of using corrosive and toxic agents for preparation.

As an important group of solvents, ionic liquids exhibit unique properties, including good dissolving ability, high ionic conductivity, extremely low volatility, and designability.[14,40,41] It has been intensively used as an environmentally benign solvent medium, especially for the organic synthesis, catalysis, and inorganic nanomaterials synthesis.[14,42−44] Ionic liquid of 1-butyl-3-methylimidazolium tetrafluoroborate ([Bmim][BF_4]) as a capping, morphology-controlling agent, and fluorine source without corrosion property provides a facile and efficient fabrication process, which makes it possible for large-scale production and morphology controllable synthesis of surface-fluorinated anatase TiO_2 nanocrystals with exposed highly active {001} facets.[14,40,45]

Herein, we successfully developed a facile strategy of ion liquid assisted etching chemistry to create TiO_2 nanocubes and TiO_2 nanocube assemblies with the surface-fluorination and nitridation and high energy {001} crystal facet exposure for improving photocatalytic performance. To achieve this, hollow TiO_2 spheres synthesized via a facile sol−gel method were hydrothermally etched with fluorine and nitrogen contained ion liquid of 1-butyl-3-methylimidazolium tetrafluoroborate without any other additives. The obtained TiO_2 nanocubes can be further assembled into hollow TiO_2 nanocube assemblies by partially connecting with the adjacent crystal facets depending on the synthetic parameters. In comparison with the TiO_2 nanostructures obtained via other synthetic strategies, the ion liquid assisted etching processes are facile and do not need any other additives, but can result in well-controlled TiO_2 nanocubes with assembling behavior and smaller size (~20 nm) due to the mild dissociation of fluorine ions from ion liquid during the etching process. The synthetic process demonstrates that the ionic liquid, acting as both a solvent and a morphology directing agent under hydrothermal etching conditions, plays a key role for the morphology evolution and surface-fluorination and nitridation of TiO_2 hierarchical architectures. The TiO_2 nanocube assemblies show very efficient photocatalytic activity for degradation of methylene blue, methyl orange, and rhodamine B under ultraviolet and visible irradiation in comparison with the TiO_2 photocatalysts adopting other morphologies and the benchmark materials of P25. The enhancement of the photocatalysis is due to the formation of active hydroxyl radicals, owing to the exposed active high energy {001} crystal facets and the surface-fluorination and nitridation. The synthetic concept via ionic liquid assisted etching chemistry to create TiO_2 hierarchical architectures with the surface-fluorination and nitridation and high energy crystal facet exposures for enhanced photocatalytic applications may provide the guidance for synthesis of other metal oxides with high energy crystal facet exposures and surface doping via chemistry method.

2. EXPERIMENTAL SECTION

Synthesis of TiO_2 Spheres. Hollow TiO_2 spheres were synthesized via a sol−gel method using SiO_2 spheres as hard scarified templates. The SiO_2 spheres were prepared by a modified Stöber method reported elsewhere.[9] The obtained SiO_2 spheres (50 mg) were dispersed into a mixture of 120 mL of ethanol and 40 mL of

acetonitrile. Then, ammonia (0.5 mL) was added. After stirring for 30 min, 1 mL of tetrabutyltitanate (TBOT) was dropped into the solution and vigorously stirred for 3 h at room temperature. Thus, the core−shell SiO_2@TiO_2 spheres were collected and washed with ethanol. The core−shell SiO_2@TiO_2 spheres were then subject to the drying at 80 °C. The hollow TiO_2 spheres were obtained by removing the SiO_2 cores via an etching process with concentrated NaOH solution. The obtained hollow TiO_2 spheres were washed with distilled water and ethanol several times and dried at 80 °C for further use.

For comparison, hollow TiO_2 spheres with well crystallized anatase phase were also prepared. The core−shell SiO_2@TiO_2 spheres were first calcined at 500 °C for 2 h in air at a heating rate of 2 °C/min to form the anatase TiO_2. Then, the SiO_2 cores were removed via an etching process with concentrated NaOH solution to obtain the anatase hollow TiO_2. The obtained hollow TiO_2 spheres were washed with distilled water and ethanol several times and dried at 80 °C for further use.

TiO_2 Nanocubes and TiO_2 Nanocube Assemblies. TiO_2 nanocubes with the exposure of {001} high energy crystal facets were prepared by a hydrothermal etching method. Hollow TiO_2 spheres (160 mg) were dispersed by ultrasonication in 40 mL of ethanol/water mixture containing 66 vol % of ethanol and 34 vol % of water. Then, ammonium fluoride (NH_4F, 0.148 g) was added. The suspension was transferred into a 50 mL Teflon-lined stainless-steel autoclave and heated at 180 °C for 20 h. After being naturally cooled down, the TiO_2 nanocubes with well-crystallized anatase phase were obtained by centrifugation and washed with distilled water and ethanol several times, and then dried at 80 °C. To monitor the growth process and morphology evolution, the experiment parameters were modulated to obtain TiO_2 with other morphologies according to Supporting Information (SI) Tables S1−S3. TiO_2 nanocube assemblies with the exposure of {001} high energy crystal facets were obtained via an ionic liquid assisted etching process by replacing the etching agent of NH_4F with an ionic liquid of 1-butyl-3-methylimidazolium tetrafluoroborate ([Bmim][BF_4]). Hollow TiO_2 spheres (80 mg) were dispersed into 10 mL [Bmim][BF_4] and 5 mL Millpore water under vigorous stirring. Then, the suspension was transferred into a Teflon-lined stainless-steel autoclave and heated at 200 °C for 20 h. After being naturally cooled down, the TiO_2 nanocube assemblies with well-crystallized anatase phase were obtained by centrifugation and washed with distilled water and ethanol several times, and then dried at 80 °C. The experimental parameters were adjusted to modulate the growth process and morphology evolution according to Scheme 1.

Characterization. Powder X-ray diffraction (XRD) was used to characterize the phase structures of TiO_2 with different morphologies. Measurements were performed using an Empyrean XRD system, PANalytical, operated at a scanning rate of 0.026° in a scanning range of 2θ = 5−80°, using Cu Kα radiation (λ = 0.154 06 Å). Samples for XRD measurements were prepared by gently crushing the obtained products with a mortar and pestle and were placed in a quartz glass holder for characterization. Scanning electron micrographs were recorded with a Hitachi S-4800 field emission scanning electron microscope (FE-SEM). Samples for SEM measurements were deposited on conductive tapes and coated with 5 nm of Pt for characterization. Transmission electron microscopy (TEM) characterization was performed on a Tecnai F20 (FEI Company) field emission transmission electron microscope system at an acceleration voltage of 120 kV to evaluate the structure, size, morphology, and exposed crystal facets of the samples. The samples for the TEM measurements were suspended in ethanol and supported onto a holey carbon film on a Cu grid. Surface area measurements were performed on an ASAP 2010 Brunauer−Emmett−Teller (BET) analyzer. The absorption spectra were recorded by a SPECORD.50 ultraviolet−visible (UV−vis) spectrophotometer (Analytikjena). Diffuse reflection spectra (DRS) of the samples were recorded on a UVIKON XL/XS spectrophotometer. The photocatalytic activity for the degradation of dye aqueous solutions was performed under a 500W Hg lamp for ultraviolet light and 500W Xe lamp for visible light (NanJing, XuJiang, SPA-7) with a cutoff filter used as a light source.

Catalytic Tests. The photocatalytic degradation of three organic dyes of methylene blue (MB), methyl orange (MO), and rhodamine B (RhB) were investigated. The catalytic tests were carried out as follows: 25 mg of the as-prepared TiO_2 catalysts were dispersed into 50 mL MB, MO, and RhB aqueous solution (2×10^{-5} mol/L), respectively. The photocatalytic activity was measured under a light of ultraviolet or visible irradiation. There is a cutoff baffle from top of analyzer. At given time intervals, about 2 mL suspension solution were sampled. The transparent solution was obtained via centrifugation to evaluate the photocatalytic activity of catalysts with the UV−visible absorption spectra.

3. RESULTS AND DISCUSSION

3.1. Synthesis, Structure, Morphology, and Configuration. The synthesis of TiO_2 nanocubes and TiO_2 nanocube assemblies in present study was carried out via a facile strategy of ionic liquid assisted etching chemistry. It is found that by etching hollow TiO_2 spheres using fluorine and nitrogen contained ionic liquid of [Bmim][BF_4] as both a solvent and an etching agent, the surface-fluorination and nitridation can be realized simultaneously without adding any other additives. Meanwhile, the ionic liquid of [Bmim][BF_4] can be also used as morphology directing agent for obtaining morphology-controlled TiO_2 nanocubes with high energy {001} crystal facets exposed. It is suggested that [Bmim][BF_4] plays a key role in the formation of anatase TiO_2 crystals with the specific facets exposed.[45] The [Bmim][BF_4] acting as a mild fluoride source is environmentally friendly and operationally safe compared with other erosive fluoride sources.[46] During the hydrothermal reaction, [Bmim][BF_4] can be disassociated into $[Bmim]^+$ and $[BF_4]^-$ ions and the $[BF_4]^-$ ions is subsequently inclined to decompose to release F^- ions.[47] It has been shown that the F^- ions are very effective in stabilizing the {001} facets of anatase TiO_2 crystals, because the surface adsorbed F^- ions are able to considerably lower the surface energy of the {001} facets, resulting in the formation of anatase TiO_2 crystals with the exposed {001} facets.[7,48]

Although previous synthetic procedures to realize the exposure of high energy crystal facets for TiO_2 photocatalysts in different morphologies have been revealed, they often involve the uses of a large amount of organic solvents, surfactant addictives, and corrosive etching agents.[7,9,10,16] To further achieve the fluorination and nitridation of TiO_2 photocatalysts, two separate synthetic processes using corrosive agents of HF and NH_4F during the synthesis for fluorination and calcining the photocatalysts in NH_3 for nitridation are commonly used.[29−36] These processes are complicated, time-consuming, and poorly environmentally benign. Therefore, the development of a strategy for simultaneously realizing the surface-fluorination and nitridation and high energy crystal facet exposure is still a big challenge and eagerly needed.

Our synthesis of TiO_2 photocatalysts with various morphologies follows the procedures shown in Scheme 1. In the synthetic strategy, hollow TiO_2 (@TiO_2) spheres composed of TiO_2 ultrafine nanoparticles, which were synthesized via a facile sol−gel method using uniform SiO_2 spheres as scarified templates,[49,50] were used as starting materials. To achieve the @TiO_2 spheres, a layer of TiO_2 was coated on SiO_2 spheres, which were obtained via a typical Stőber method to form core−shell SiO_2@TiO_2 spheres. Then, the SiO_2 templates were removed by etching with concentrated NaOH solution to achieve @TiO_2 spheres. Starting from the @TiO_2 spheres, TiO_2 photocatalysts with different hierarchical architectures were obtained via an etching chemistry process

with ionic liquid of [Bmim][BF_4] or nonionic liquid agent of NH_4F.

Figure 1 shows the SEM and TEM images of SiO_2@TiO_2 and @TiO_2 spheres after etching with NaOH solution. The

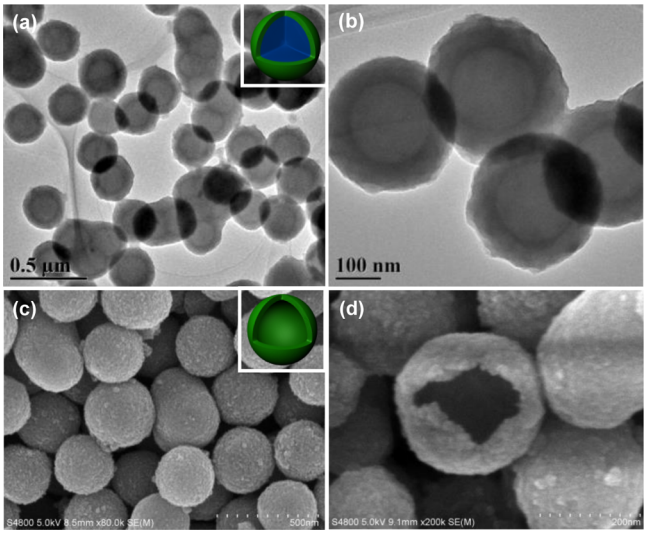

Figure 1. TEM images of (a and b) SiO_2@TiO_2 and SEM images of (c and d) @TiO_2 spheres for creating TiO_2 photocatalysts with various morphologies. The insets in parts a and d show the schematic diagrams of SiO_2@TiO_2 and @TiO_2 spheres.

SiO_2 spheres possess good uniformity and monodispersity with average sizes of ~200 nm and are used as scarified templates. After coating a layer of TiO_2, the SiO_2@TiO_2 spheres maintain the similar uniformity and monodispersity (Figure 1a,b). By etching with NaOH solution, uniform @TiO_2 spheres with a shell thickness of ~40 nm are obtained (Figure 1c,d). The @TiO_2 spheres are used as starting TiO_2 precursors for creating TiO_2 photocatalysts with various hierarchical architectures via a hydrothermal etching process.

To develop a strategy for synthesizing TiO_2 photocatalysts with high energy crystal facet exposures, an ionic liquid assisted etching process was adopted using the ionic liquid of [Bmim][BF_4] as fluorine and nitrogen source, solvent, and morphology directing agent. By hydrothermally etching, the @TiO_2 spheres in the presence of [Bmim][BF_4] with the existence of a small amount of EtOH and H_2O, TiO_2 nanocubes with high energy {001} crystal exposure were obtained (S1 in Scheme 1 and L1 in SI Table S1), as shown in Figure 2. The obtained TiO_2 nanocubes are uniform and monodispersed (Figure 2a,b) and most of them adopt cubic shapes with an average diameter of ~30 nm smaller than previous reports for TiO_2 nanocubes synthesized via other approaches.[45] The TEM and HRTEM images reveal that apart from the TiO_2 nanocubes (marked with red circle in Figure 2c), TiO_2 hexahedrons are also observed (marked with white circle in Figure 2c). The HRTEM image shows that the TiO_2 nanocubes have the high energy {001} crystal facets exposed (Figure 2d). Comparatively, when solely using the ionic liquid of [Bmim][BF_4] with the existence of a small amount of H_2O for hydrothermal treatment, the TiO_2 nanocubes (S2 in Scheme 1 and L2 in SI Table S1) with high energy {001} crystal facets exposed can be also obtained, however, they tend to assemble into hollow hierarchical architecture, as shown in Figure 3. The time-dependent experiments prove that even in a

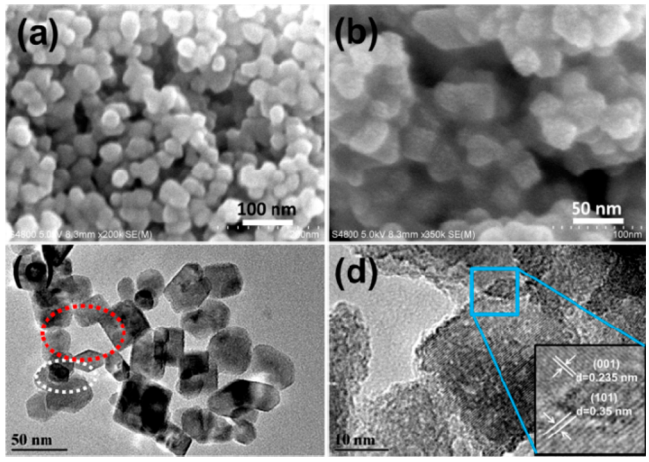

Figure 2. SEM (a and b), TEM (c), and HRTEM (d) images of TiO_2 nanocubes with the exposure of high energy {001} crystal facets synthesized by hydrothermally treating @TiO_2 at 200 °C for 20 h in mixed solvents of 5 mL of [Bmim][BF_4], 5 mL of EtOH, and 5 mL of H_2O. The white and red circles in part c indicate the TiO_2 nanocubes and hexahedrons are formed.

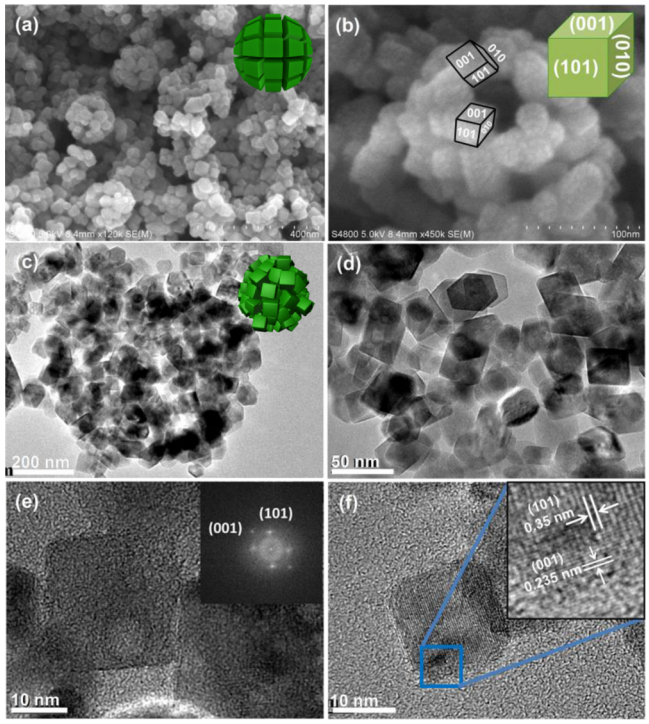

Figure 3. SEM (a and b), TEM (c and d), and HRTEM (e and f) images of TiO_2 nanocube assemblies synthesized by hydrothermally treating @TiO_2 at 200 °C for 20 h in mixed solvents of 10 mL of [Bmim][BF_4] and 5 mL of H_2O. The insets in parts a–c show schematic diagrams of TiO_2 nanocube and nanocube assemblies. The insets in parts e–f indicate the SAED pattern and the HRTEM image of connecting crystal facets for adjacent TiO_2 nanocubes.

short reaction period of 10 h, the TiO_2 nanocube assemblies can be formed (SI Figure S1). With the prolong of the reaction time, the TiO_2 nanocube assemblies gradually become larger, confirming the formation of hierarchical architecture TiO_2 assembled from TiO_2 nanocubes. The TiO_2 nanocube assemblies have an average size of ~180 nm and are assembled into hollow architecture composed of unique TiO_2 nanocubes

by connecting the adjacent crystal plane (Figure 3a–d). The TiO_2 nanocubes have the exposed crystal facets of {001}, {010}, and {101} (Figure 3b,e–f). The SAED exhibits sharp diffraction spots ascribed to the {101} lattice plane, suggesting that the nanocubes possess the crystal facets of {001}, {010}, and {101}. The reflections with *d* spacing values of 0.235 and 0.35 nm are obviously observed (Inset in Figure 3f), which are well indexed to the {001} and {101} lattice planes of anatase TiO_2, respectively. The TiO_2 nanocubes are connected with the adjacent {101} lattice plane to form the nanocube assemblies. In comparison with the hydrothermal treatment for obtaining TiO_2 nanocube assemblies using H_2O as solvent, the hydrothermal treatment for using EtOH as solvent can only lead to the formation of TiO_2 nanocubes. This may be ascribed to weak interaction between hydroxyl groups on TiO_2 surface and EtOH. It is speculated that due to the large amount of hydroxyl groups existing on the surface of TiO_2 nanocubes, the TiO_2 nanocubes may have a strong interaction with H_2O by forming the hydrogen bond when using H_2O as the reaction solvent, which may cause the TiO_2 nanocubes liable to be developed into nanocube assemblies. However, when using the mixed solvent of H_2O and EtOH as reaction medium, the interaction of the hydrogen bond between hydroxyl groups on the TiO_2 surface and EtOH is weakened because of the alkyl groups introduced by EtOH. Thus, the TiO_2 nanocubes may be less liable to form TiO_2 nanocube assemblies.[45]

It is found that the hydrothermal treatment and the solvent are crucial for achieving TiO_2 photocatalysts with cubic shape. When the ionic liquid assisted etching process is carried out in a pure ionic liquid of $[Bmim][BF_4]$ without addition of other solvents of H_2O and EtOH either in atmosphere or under hydrothermal condition (L3 and L4 in SI Table S1), only @TiO_2 spheres composed of well-crystallized ultrafine TiO_2 nanoparticles (~10 nm) can be obtained even the treatment temperature is raised to 300 °C in atmosphere (SI Figures S3 and S4). The obtained @TiO_2 spheres have very loose hollow structures with the porous shells, which could be used as microreactors for photocatalytic application.

It was reported that the ionic liquid of $[Bmim][BF_4]$ can be used as a morphology-directing agent for synthesis of TiO_2 crystals with various morphologies.[45] However, without the addition of other solvents such as H_2O and EtOH, the $[Bmim][BF_4]$ alone is not liable to dissociate into $[Bmim]^+$ and $[BF_4]^-$ and subsequently to release F^- ions under hydrothermal conditions due to its high boiling point. Thus, without the dissociated F^- ions in the reaction system, the morphology of TiO_2 crystals seems not to change too much. However, when there exists the H_2O and EtOH, the dissociation of $[Bmim][BF_4]$ and the release of F^- ions are much easier, and the dissociated F^- ions may largely affect the morphology of TiO_2 crystals, as the F^- ions are very effective in stabilizing the {001} facets of anatase TiO_2 crystals by absorbing on their surface to lower the surface energy of the {001}.[46−48] Similarly, the NH_4F may also act as a morphology-directing agent for synthesis of TiO_2 crystals with various morphologies and follows the similar mechanism.

To explore the morphology-directing capability of ionic liquids, the etching chemistry process was also carried out for comparison by using nonionic liquid agent NH_4F to replace the ionic liquid of $[Bmim][BF_4]$. It is shown that TiO_2 photocatalysts with different morphologies of hollow spheres, cubes, hollow flaky spheres, and spindles can be formed as shown in Figures 4 and 5. It is suggested that the amounts of etching

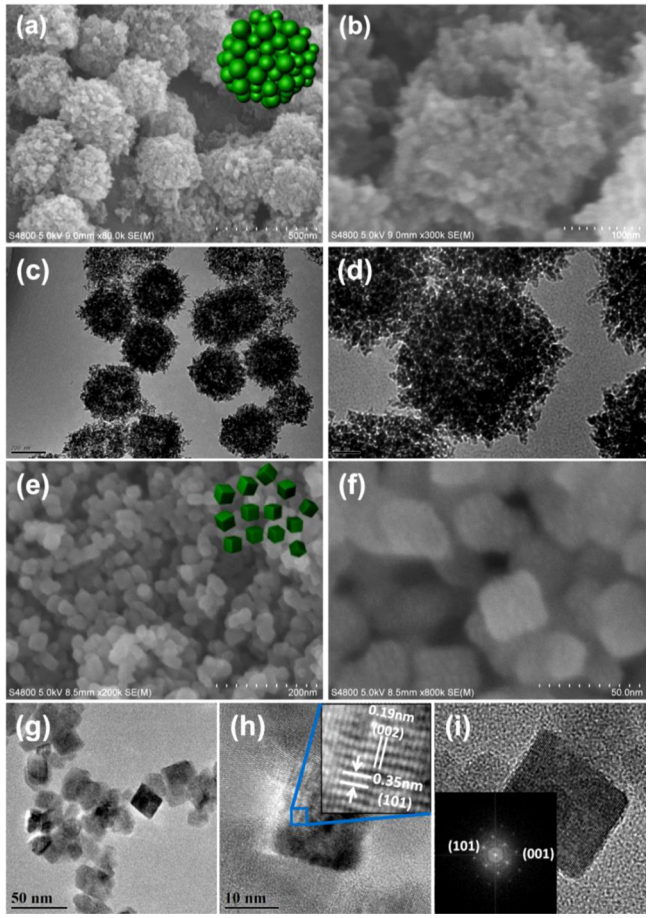

Figure 4. SEM (a, b, e, and f), TEM (c and d), and HRTEM (g, h, and i) images of (a–d) @TiO_2 spheres composed of ultrafine TiO_2 nanoparticles and (e–i) TiO_2 nanocubes obtained by hydrothermally treating @TiO_2 spheres with the molar ratio of @TiO_2 to NH_4F at 1:2 at 180 °C for different times in a mixed solvent of EtOH and H_2O according to SI Table S2. The insets in a and e display the schematic diagrams of TiO_2 hollow spheres and nanocubes. The insets in h and I present the HRTEM image and SAED pattern for exposure of TiO_2 nanocubes.

agent of NH_4F have significant impacts on the morphology and configuration of TiO_2 photocatalysts. Meanwhile, it is found that the TiO_2 obtained via hydrothermal etching treatment at 200 or 180 °C has no significant variation in morphology when using NH_4F as morphology directing agent for the synthesis. Thus, the reaction temperature was kept for all synthesis. When using higher amounts of NH_4F as etching agent (molar ratio of @TiO_2 to NH_4F = 1:2 according to SI Table S2), well crystallized @TiO_2 spheres (S3 in Scheme 1) is formed within a short period of hydrothermal etching time (0.5–10 h) (Figure 4a–d and SI Figure S5). The @TiO_2 spheres are assembled by ultrafine TiO_2 nanoparticles (~10 nm) and show obvious hollow structures. When keeping other etching conditions identical but increasing, the hydrothermal etching time to 15–20 h, TiO_2 nanocubes (S4 in Scheme 1) are achieved (Figure 4e,f). The TiO_2 nanocubes are uniform and have a cubic shape with an average size of ~20 nm. The HRTEM images (Figure 4g–h) show that the TiO_2 nanocubes are well crystallized and the reflection distances of 0.19 and 0.35 nm corresponding to the (002) and (101) crystal lattices of anatase TiO_2 are clearly observed (inset in Figure 4h), suggesting that anatase TiO_2 spheres are formed after

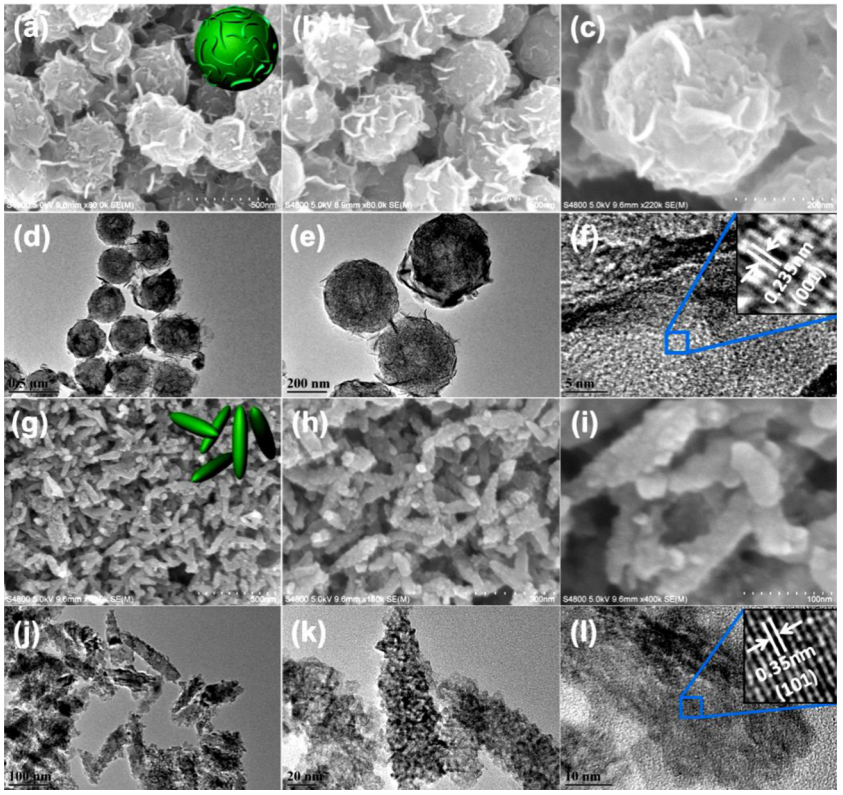

Figure 5. SEM (a, b, c, g, h, and i), TEM (d, e, j, and k), and HRTEM (f and l) images of (a–f) flaky @TiO_2 spheres and (g–l) TiO_2 nanospindles obtained by hydrothermally treating @ TiO_2 spheres with different molar ratio of @ TiO_2 to NH_4F at 180 °C for 4 h in a mixed solvent of EtOH and H_2O according to SI Table S3. The insets in a and g display the schematic diagrams of TiO_2 hollow flaky spheres and nanospindles. The insets in f and l indicate the HRTEM image of TiO_2 flakes and spindles.

hydrothermal treatment of amorphous @TiO_2 spheres. Combining with the SAED results shown in the inset in Figure 4i, it is revealed that the TiO_2 nanocubes have the high energy {001} crystal facets exposed, which is proven to be highly active for photocatalysis.

Changing the etching agent to a very lower amount of NH_4F (molar ratio of @TiO_2 to NH_4F = 10:1 according to SI Table S3) and keeping the hydrothermal etching time at 4 h, flaky @ TiO_2 spheres (S5 in Scheme 1) are synthesized. The flaky @ TiO_2 spheres are very uniform and maintain a hollow configuration, but have a large amount of flaky TiO_2 on the surface of TiO_2 spheres due to the soft etching with the low concentration of NH_4F under hydrothermal conditions (Figure 5a–c). The flaky @TiO_2 spheres are estimated to be ~200 nm with thin TiO_2 flakes (~20 nm in thickness) on the surface. The thin TiO_2 flakes cover the whole surface of TiO_2 spheres (Figure 5d,e). The TiO_2 flakes growing along the (001) lattice plane are well discerned (Figure 5f) as the reflection distance of 0.235 nm indexed to the (001) lattice plane are clearly observed. A little bit increasing the amount of etching agent of NH_4F (molar ratio of @TiO_2 to NH_4F = 2.5:1 according to SI Table S3) but still lower than that used for preparing @TiO_2 spheres and TiO_2 nanocubes, uniform TiO_2 nanospindles (S6 in Scheme 1) are obtained (Figure 5g–l). The obtained TiO_2 nanospindles are composed of ultrafine TiO_2 nanoparticles (Figure 5j,k), which are assembled into spindle morphology along the (001) growth direction (Figure 5l and inset).

To further confirm the phase structure of the obtained TiO_2 nanostructures, XRD characterization was carried out, which is shown in Figures 6 and SI Figures S6–S8. It is revealed that all

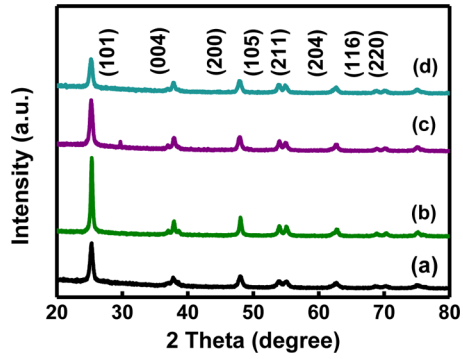

Figure 6. XRD patterns of (a) commercial benchmark materials of P25, (b) @TiO_2 spheres calcined at 500 °C, (c) TiO_2 nanocubes obtained by etching @TiO_2 spheres with NH_4F, and (d) TiO_2 nanocube assemblies synthesized by etching @TiO_2 spheres with ionic liquid of [Bmim][BF_4].

obtained TiO_2 with various morphologies are well crystallized after hydrothermal treatment (SI Figures S6–S8). The hydrothermal treatment in different conditions has great impact on the particle size and morphology. Figure 6 shows the typical XRD patterns of benchmark materials of P25, @TiO_2 spheres calcined at 500 °C, TiO_2 nanocubes obtained by etching with NH_4F, and TiO_2 nanocube assemblies achieved by etching with [Bmim][BF_4], respectively. According to the XRD patterns, all the obtained TiO_2 photocatalysts are in anatase phase with high crystallization degree (JCPDS 21-1272). The characteristic diffraction peaks located at 25°, 38°, 48°, 54°, 55°, 63°, 69°, 70°, and 75° can be well indexed to the lattice planes of (101),

(004), (200), (105), (211), (204), (116), (220), and (205) of anatase phase TiO_2 nanostructures. A small diffraction peak appeared at 29° can be observed for TiO_2 nanocubes and nanocube assemblies [Figures 6(c) and S6(L2)], which may be assigned to the formation of $TiOF_2$ due to the F^- ion doping by partially substituting of O^{2-}.[51] The crystallite sizes along the [001] and [101] axes vertical to (001) and (101) crystal facets exhibit a much higher percentage of exposed (001) crystal facets for TiO_2 nanocube and TiO_2 nanocube assemblies than @TiO_2 spheres and P25, resulting in the higher photocatalytic property.[52] The average size of TiO_2 photocatalysts are be evaluated to be 18.3, 24.4, 17.8, and 15.8 nm for P25, @TiO_2 spheres calcined at 500 °C, TiO_2 nanocubes obtained by etching with NH_4F, and TiO_2 nanocube assemblies achieved by etching with [Bmim][BF_4], respectively, according to show relatively smaller particle sizes in comparison to @TiO_2 spheres (SI Table S4).

3.2. PHYSICOCHEMICAL PROPERTY

To explore the surface area and pore-size distribution of the obtained TiO_2 photocatalysts with various morphologies, the

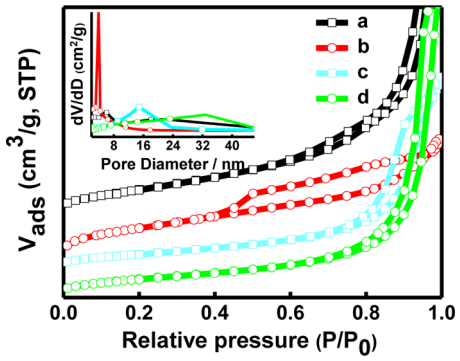

Figure 7. N_2 absorption and desorption isomers and BJH measurement (inset) of (a) commercial benchmark materials of P25, (b) @TiO_2 spheres calcined at 500 °C, (c) TiO_2 nanocubes obtained by etching @TiO_2 spheres with NH_4F, and (d) TiO_2 nanocube assemblies synthesized by etching @TiO_2 spheres with ionic liquid of [Bmim][BF_4].

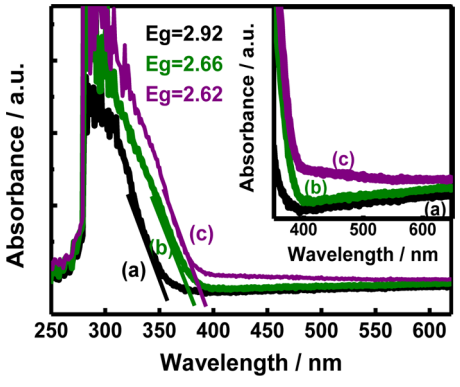

Figure 8. UV−visible diffuse reflectance spectra of (a) @TiO_2 spheres calcined at 500 °C, (b) TiO_2 nanocubes obtained by etching @TiO_2 spheres with NH_4F, and (c) TiO_2 nanocube assemblies synthesized by etching @TiO_2 spheres with ionic liquid of [Bmim][BF_4]. The inset shows the magnified UV−visible diffuse reflectance spectra in visible light range.

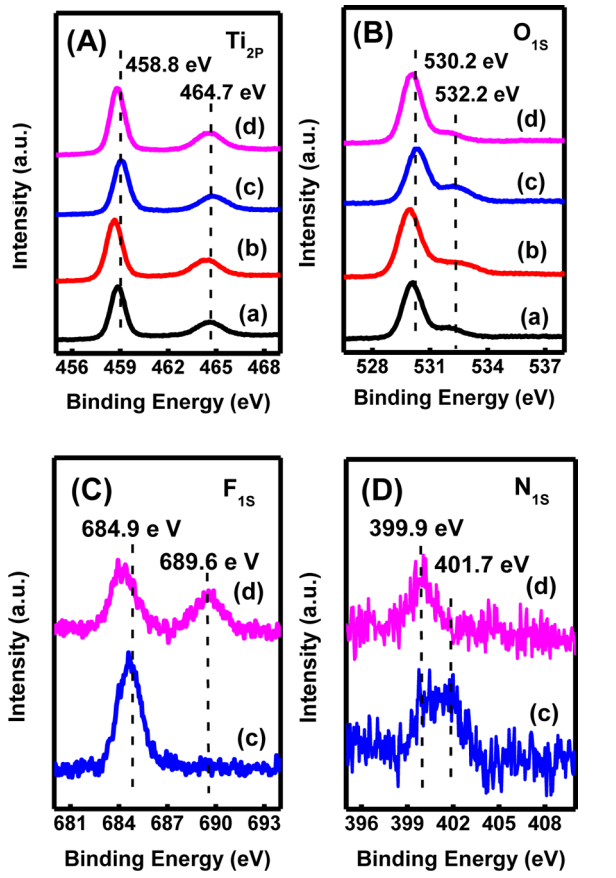

Figure 9. Fine XPS spectra of (A) Ti2p, (B) O1s, (C) F1s, and (D) N1s of (a) commercial benchmark materials of P25, (b) @TiO_2 spheres calcined at 500 °C, (c) TiO_2 nanocubes obtained by etching @TiO_2 spheres with NH_4F, and (d) TiO_2 nanocube assemblies synthesized by etching @TiO_2 spheres with ionic liquid of [Bmim][BF_4].

BET characterization was conducted (Figure 7 and SI Table S4). Figure 7 shows the nitrogen adsorption−desorption isotherms and the corresponding pore-size distribution of commercial benchmark materials of P25, @TiO_2 spheres calcined at 500 °C, TiO_2 nanocubes obtained by etching with NH_4F, and TiO_2 nanocube assemblies achieved by etching with [Bmim][BF_4]. The isotherms exhibit the type IV characteristics of a type H1 for P25, @TiO_2 spheres calcined at 500 °C, and TiO_2 nanocube assemblies achieved by etching with [Bmim]-[BF_4] (Figure 7a,b,d) and H2 hysteresis loop for TiO_2 nanocubes obtained by etching with NH_4F (Figure 7c),[52] giving the evidence that @TiO_2 spheres and TiO_2 nanocube assemblies possess the mesoporous characteristics with assembling behavior. The hysteresis loop for TiO_2 nanocubes appeared in the relative pressure (P/P_0) range of 0.7−1.0 suggests the existence of large mesopores and macropores resulted from the aggregation of nanocubes, which also can be clearly seen in SEM image (Figure 4e,f). TiO_2 nanocube assemblies present a hysteresis loop of type IV isotherm over a range of high P/P_0 from 0.8 to 1.0, which is associated with capillary condensation taking place in mesopores. The initial part of the isotherm is attributed to monolayer-multilayer adsorption. As we know, type IV isotherms are given by many mesoporous industrial adsorbents.[53] As the pore size distribution in quite wide range of 0 to 30 nm is observed, the aggregated TiO_2 porous structures are considered to be

dx.doi.org/10.1021/am5016809 | ACS Appl. Mater. Interfaces 2014, 6, 10283−10295

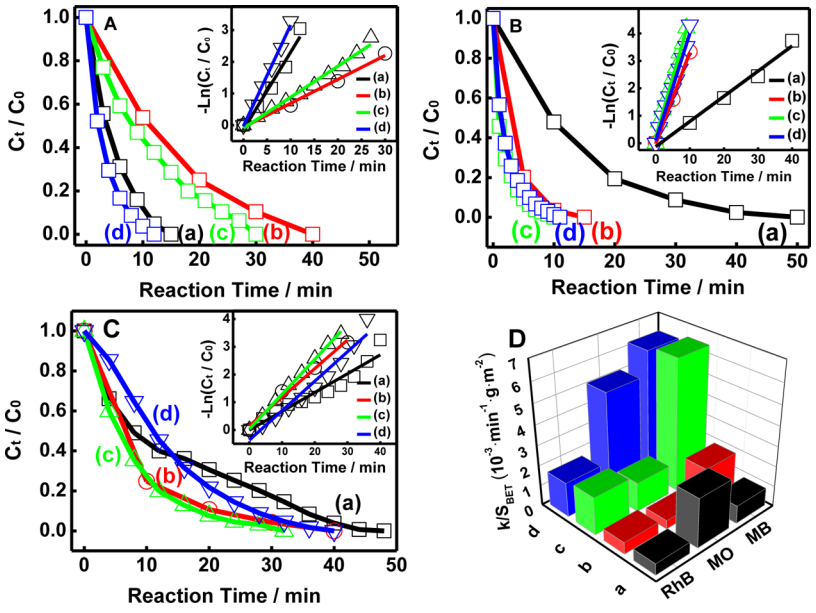

Figure 10. Degradation rates of (A) MO, (B) MB, and (C) RhB aqueous solutions against the reaction time under ultraviolet light irradiation in the presence of (a) commercial benchmark materials of P25, (b) @TiO_2 spheres calcined at 500 °C, (c) TiO_2 nanocubes obtained by etching @TiO_2 spheres with NH_4F, and (d) TiO_2 nanocube assemblies synthesized by etching @TiO_2 spheres with ionic liquid of [Bmim][BF_4], and (D) space diagram of normalized reaction rate constants for (a) P25, (b) @TiO_2 spheres, (c) TiO_2 nanocubes, and (d) TiO_2 nanocube assemblies.

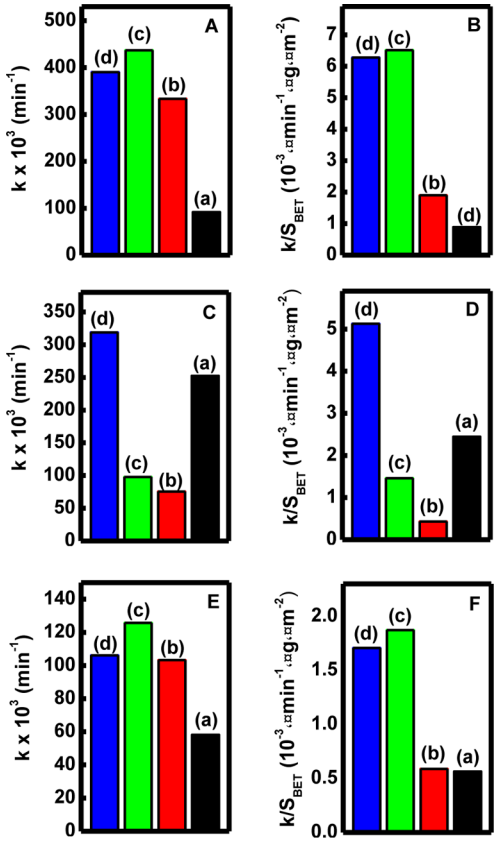

Figure 11. Reaction rate constants and normalized reaction rate constants of different photocatalysts for degradation of (A and B) MO, (C and D) MB, and (E and F) RhB on various photocatalysts of (a) commercial benchmark materials of P25, (b) @TiO_2 spheres calcined at 500 °C, (c) TiO_2 nanocubes obtained by etching @TiO_2 spheres with NH_4F, and (d) TiO_2 nanocube assemblies synthesized by etching @TiO_2 spheres with ionic liquid of [Bmim][BF_4].

extremely useful in photocatalysis. They may provide flexible transport pathways for the diffusion of reactants during the photocatalytic process.

To further verify the influences of the morphology variation and assemble behavior on their absorbance property, the UV−visible diffuse reflectance spectra (UV−vis DRS) of @TiO_2 spheres calcined at 500 °C, TiO_2 nanocubes obtained by etching with NH_4F, and TiO_2 nanocube assemblies achieved by etching with [Bmim][BF_4] were recorded, as shown in Figure 8. It can be seen clearly that the UV−visible absorption for TiO_2 photocatalysts with various morphologies is varied and a wider absorption region close to visible light region is realized for TiO_2 nanocubes and TiO_2 nanocube assemblies in comparison to @TiO_2 spheres. In addition, the light absorbance in UV−visible range of 200 to 320 nm is varied in the order of TiO_2 nanocube assemblies > TiO_2 nanocubes> @TiO_2 spheres corresponding to the band gap order, and there is an obviously different band gap value, which may be due to the improved percentage of exposed high energy crystal facets.[14−16] According to the intensities of the (004) and (101) diffraction peaks, it is calculated that the intensity ratio of (004) to (101) planes are 0.257 for nanocubes and 0.335 for nanocube assemblies, suggesting the higher value of the percentage of exposed high energy crystal facets for TiO_2 nanocube assemblies. Furthermore, it was observed that compared with the bare @TiO_2 spheres, the TiO_2 nanocubes obtained by etching @TiO_2 spheres with NH_4F and TiO_2 nanocube assemblies obtained by etching @TiO_2 spheres with [Bmim][BF_4] show the obvious visible light response in the visible light region of 400−650 nm due to the N doping (inset in Figure 8).[5]

To identify the surface element composition and the valence state of TiO_2 photocatalysts with various morphologies on their photocatalytic properties, XPS characterization of Ti, O, F, and N elements in commercial benchmark materials of P25, @TiO_2 spheres calcined at 500 °C, TiO_2 nanocubes obtained by etching with NH_4F, and TiO_2 nanocube assemblies achieved by

dx.doi.org/10.1021/am5016809 | ACS Appl. Mater. Interfaces 2014, 6, 10283−10295

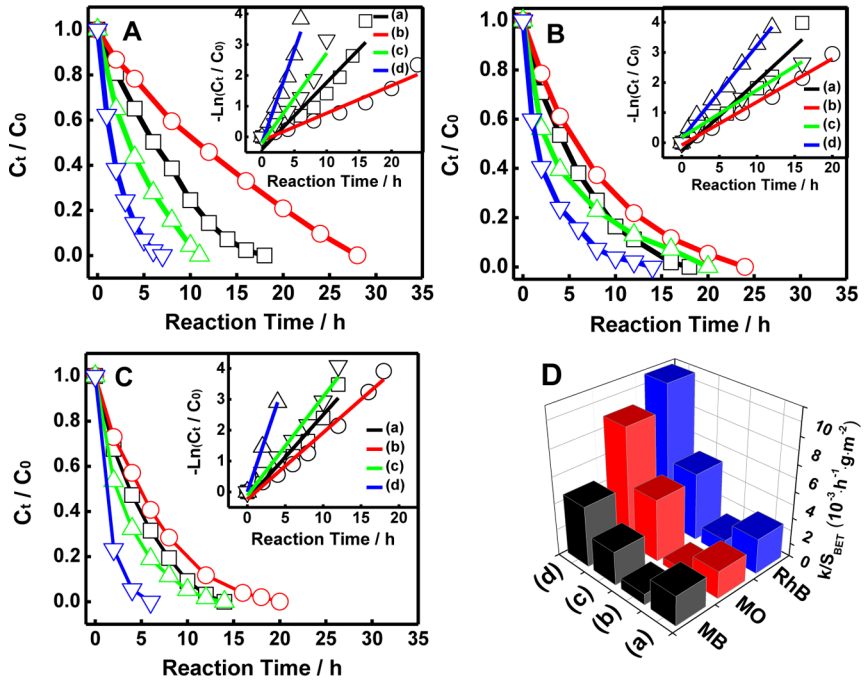

Figure 12. Degradation rates of (A) MO, (B) MB, and (C) RhB aqueous solutions against the reaction time under visible light irradiation in the presence of (a) commercial benchmark materials of P25, (b) @TiO_2 spheres calcined at 500 °C, (c) TiO_2 nanocubes obtained by etching @TiO_2 spheres with NH_4F, and (d) TiO_2 nanocube assemblies synthesized by etching @TiO_2 spheres with ionic liquid of [Bmim][BF_4], and (D) space diagram of normalized reaction rate constants for (a) P25, (b) @TiO_2 spheres, (c) TiO_2 nanocubes, and (d) TiO_2 nanocube assemblies.

etching with [Bmim][BF_4] were carried out, which are shown in Figure 9. The XPS results clearly indicate that Ti and O elements all appear in all catalysts but F and N elements exist in TiO_2 nanocubes and TiO_2 nanocube assemblies, as their characteristic XPS peaks can be well assigned to Ti_{2p} (458.8 and 464.7 eV), O_{1s} (530.2 and 532.2 eV), F_{1s} (684.9 and 689.6 eV), and N_{1s} (399.9 and 401.7 eV). However, based on the surface-fluorination and nitridation with different agents of NH_4F and [Bmim][BF_4], the binding energies for Ti_{2p}, O_{1s}, F_{1s}, and N_{1s} elements in TiO_2 nanocubes and TiO_2 nanocube assemblies are slightly varied in comparison with P25 and @TiO_2 spheres. This suggests that the etching chemistry of @TiO_2 spheres with fluorine- and nitrogen-containing agents plays a key role in realizing the surface-fluorination and nitridation of TiO_2 photocatalysts. The etching process carried out using different etching agents of NH_4F and [Bmim][BF_4] may cause the slight shift of binding energy of Ti_{2p} and O_{1s} (Figure 9A,B), implying that the valence status of Ti and O in the photocatalysts is varied, which may lead to the variation of their catalytic performance.[31,45] Compared with the binding energies of Ti_{2p} for P25, the binding energies for @TiO_2 spheres, @TiO_2 nanocubes, and TiO_2 nanocube assemblies slightly shift to lower binding energy region, suggesting the formation of Ti^{3+} due to the hydrothermal treatment with concentrated NaOH solution for @TiO_2 spheres and the doping of F and N for @TiO_2 nanocubes and TiO_2 nanocube assemblies.[19,54] Meanwhile, the formation of hydroxide groups on the surface of TiO_2 causes the slight shift of O binding energy to lower region.[19,54] The XPS peak of F_{1s} with the binding energy located at 684.9 eV, which can be assigned to the typical value of F^- in fluorine TiO_2 system such as Ti−F species,[7] can be clearly observed (Figure 9C), suggesting the successful realization of surface doping of F^- ion in the crystal surface of TiO_2 nanocubes and TiO_2 nanocube assemblies. In contrary, no XPS peak related to F^- ion is found in commercial benchmark materials of P25 and @TiO_2 spheres. Moreover, an additional XPS peak located at 689.6 eV is also observed (Figure 9C), which may be associated with the F^- ions in $[BF_4]^-$ ions that absorb on the surface of TiO_2 nanocube assemblies.[45−48] In contrast, no similar peak is observed for TiO_2 nanocubes, as free F^- ion come from NH_4F has less absorptive ability and can be easily removed. The XPS signal from N_{1s} further prove the realization of surface-nitridation (Figure 9D), however, due to the surface-nitridation occurs using different N source agents of NH_4F and [Bmim][BF_4], the binding energy of N_{1s} in TiO_2 nanocube assemblies shifts to lower range compared to that in TiO_2 nanocubes.[55,56] Such results strongly suggest that the etching with NH_4F or [Bmim][BF_4] can result in the surface-fluorination and nitridation of TiO_2 photocatalysts in addition to realizing the high energy crystal facet exposure. However, according to different etching agents, the valence status of Ti and O and the surface doping state of F and N may be varied, which may cause the discrepancy on their catalytic activity.

3.3. Photocatalytic Performance. Because of the surface-fluorination and nitridation and the exposure of high energy crystal facets, the obtained TiO_2 nanocubes and TiO_2 nanocube assemblies are expected to have highly efficient catalytic activity. Meanwhile, the TiO_2 nanocube assemblies in hollow spherical configuration with a confinement central environment may be used as effective microreactors for photocatalytic applications and expect to have a higher photocatalytic activity.[36,49,50] The photocatalytic degradation of organic dyes of methyl orange (MO), methylene blue (MB), and rhodamine B (RhB) under UV and visible light radiation at room temperature were used to evaluate the photocatalytic activity of TiO_2 photocatalysts with various morphologies. Figures 10−13 shows a contra-distinction in photocatalytic degradation of MO, MB, and RhB on various TiO_2 photocatalysts of commercial benchmark

dx.doi.org/10.1021/am5016809 | ACS Appl. Mater. Interfaces 2014, 6, 10283−10295

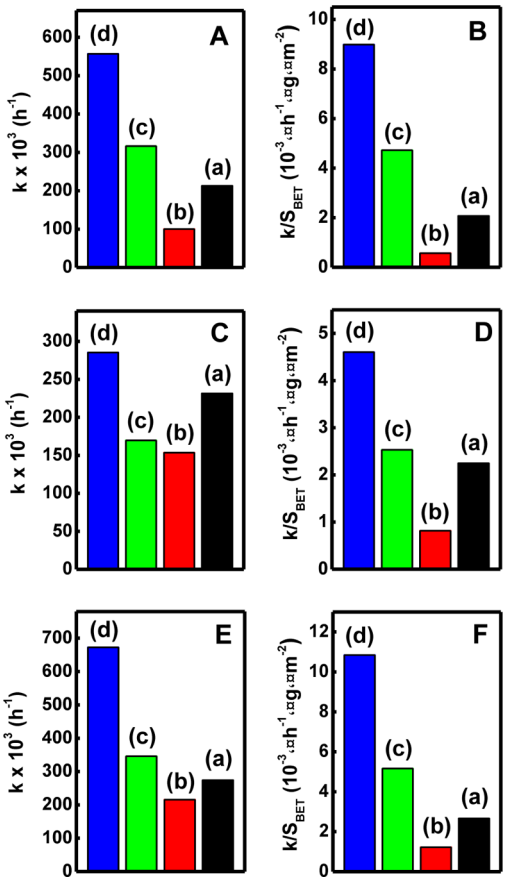

Figure 13. Reaction rate constants and normalized reaction rate constants of different photocatalysts for degradation of (A and B) MO, (C and D) MB, and (E and F) RhB on various photocatalysts of (a) commercial benchmark materials of P25, (b) @TiO_2 spheres calcined at 500 °C, (c) TiO_2 nanocubes obtained by etching @TiO_2 spheres with NH_4F, and (d) TiO_2 nanocube assemblies synthesized by etching @TiO_2 spheres with ionic liquid of [Bmim][BF_4].

materials of P25, @TiO_2 spheres calcined at 500 °C, TiO_2 nanocubes obtained by etching with NH_4F, and TiO_2 nanocube assemblies achieved by etching with [Bmim][BF_4]. Comparing with the benchmark materials of P25, @TiO_2 spheres, and TiO_2 nanocubes, the TiO_2 nanocube assemblies with surface-fluorination and nitridation and high energy {001} crystal facets exposed display improved photocatalytic activity for degradation of various organic dyes of MO, MB, and RhB. The changes of absorption spectra at major absorption bands for MO, MB, and RhB solutions and the color changes of MO, MB, and RhB dye degraded with P25, @TiO_2 spheres, TiO_2 nanocube, and TiO_2 nanocube assemble photocatalysts after different time intervals indicate that the chromophoric structure of MO, MB, and RhB is destroyed due to photocatalytic degradation (Figures 10 and 12). The TiO_2 nanocube assemblies show the fastest degradation rate in comparison to other photocatalysts of P25, @TiO_2 spheres, and TiO_2 nanocubes. On the basis of the degradation species, the TiO_2 nanocube assemblies show slight discrepancy in degradation efficiency (Figures 11 and 13), however, it shows super high catalytic efficiency on the degradation of organic dyes of MO, MB, and RhB in comparison with P25, @TiO_2 spheres, and TiO_2 nanocubes. The overall photocatalytic activity in per unit surface area of TiO_2 nanocube assemblies is much higher than the P25, @TiO_2 spheres, and TiO_2 nanocubes. The reaction rate constants and normalized reaction rate constants of for the degradation of organic dyes of MO, MB, and RhB are much higher as well.

To study the recyclability of the TiO_2 nanocubes and TiO_2 nanocube assemblies, the recyclability tests of degradation of RhB on TiO_2 nanocubes and TiO_2 nanocube assemblies under ultraviolet-light irradiation were carried out and the results are shown in SI Figures S9 and S10. It is found that the photocatalytic performance of TiO_2 nanocube assemblies shows a 65% degradation rate of RhB after 5 cycle running, which is better than the photocatalytic performance of TiO_2 nanocubes with a 32% degradation rate after 5 cycle running. This suggests that TiO_2 nanocube assemblies may have better photocatalytic stability than TiO_2 nanocubes.

It is reported that high energy {001} crystal facets of anatase TiO_2 photocatalysts may induce to generate more electron–hole pairs, which tends to combine with hydrogen peroxide (H_2O_2) in aqueous solution and cause the hydrogen peroxide dissociated to produce hydroxyl radical (•OH) (Scheme 2).[57,58] Large amounts of hydroxyl radicals are responsible for rapid degradation of dye molecules.[57−59] Meanwhile, the surface-fluorination and nitridation may also cause the electron-balance, leading to the generation of defects. Therefore, the enhanced photocatalytic degradation of dye molecules can be realized by optimizing the TiO_2 photocatalytic property through a strategy to make the high energy crystal facets of TiO_2 exposed using ionic liquid of [Bmim][BF_4] as an etching agent under hydrothermal conditions. Because of its high thermal stability, the ionic liquid of [Bmim][BF_4] has a slower desiccation rate to release F^- ions, which makes the etching process take place slower, and favors the formation of TiO_2 nanocube assemblies.

4. CONCLUSIONS

A facile strategy of ionic liquid assisted etching chemistry was developed to create highly active anatase TiO_2 nanocubes and TiO_2 nanocube assemblies. This approach was carried out by hydrothermally etching @TiO_2 spheres with fluorine and

Scheme 2. Mechanism of Catalytic Performance of TiO_2 Nanocube Assemblies for Enhanced Catalytic Degradation of MB, MO, and RhB

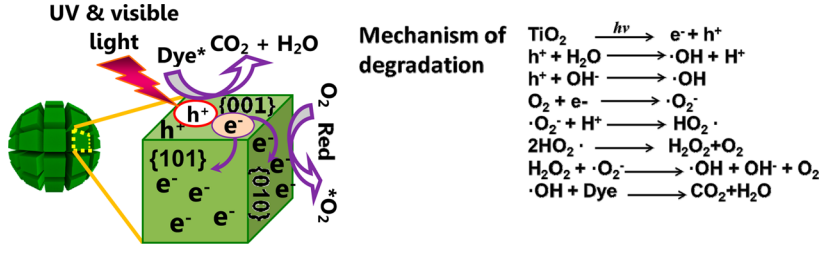

nitrogen contained ionic liquid of [Bmim][BF_4], resulting in the realization of surface-fluorination and nitridation and high energy {001} crystal facet exposure simultaneously. In comparison to the TiO_2 nanostructures with other morphologies of hollow spheres, flaky spheres, and spindles synthesized with the similar etching chemistry but using nonionic liquid NH_4F as an etching agent, the etching process is quite mild due to the slow dissociation of fluorine ions released from an ionic liquid, thus leading to the formation of TiO_2 nanocube assemblies by connecting with the adjacent crystals facets. The TiO_2 nanocubes and nanocube assemblies can be used as effective photocatalysts for enhanced photocatalytic degradation of organic dyes of MO, MB, and RhB due to the surface-fluorination and nitridation and the exposure of high energy {001} crystal facets. A significant improvement in photocatalytic degradation of organic dyes can be realized in TiO_2 nanocubes and TiO_2 nanocube assemblies in comparison to the benchmark materials of P25. The surface-fluorination and nitridation and the exposure of high energy {001} crystal facets, which may induce more electron−hole pairs beneficial to form hydroxyl radical and extend the spectral response range with higher absorbance ability, are proposed to account for the enhancement of their photocatalytic property for organic dyes degradation. Meanwhile, the hollow microreactor configuration of TiO_2 nanocube assemblies with the confinement effect could also provide transport pathways for the diffusion of reactants and products during organic dye degradation process, which physically improves the photocatalytic degradation of organic dyes as well. The obtained TiO_2 photocatalysts with various shapes, morphologies, and configurations in this study may find potential applications in photocatalysis. The ionic liquid assisted etching chemistry is facile and robust and can be a general strategy for creating other metal oxides in an assembled configuration with the exposure of high energy crystal facets and surface doping to improve their photocatalytic activity.

■ ASSOCIATED CONTENT

Ⓢ Supporting Information

Tables summarizing reaction conditions and morphologies, XRD, BET, and SEM characterization. This material is available free of charge via the Internet at http://pubs.acs.org.

■ AUTHOR INFORMATION

Corresponding Author

*E-mail: cejzhang@imu.edu.cn.

Notes

The authors declare no competing financial interest.

■ ACKNOWLEDGMENTS

This work was supported by NSFC (21261011), Program for New Century Excellent Talents in University (NCET-10-0907), Application Program from Inner Mongolia Science and Technology Department (113307), Inner Mongolia Public Security Program (208096), Inner Mongolia "Grassland" Talent, and Inner Mongolia Talent development Funding.

■ REFERENCES

(1) Fujishima, A.; Honda, K. Electrochemical Photolysis of Water at a Semiconductor Electrode. *Nature* **1972**, *238*, 37−38.

(2) Grätzel, M. Photoelectrochemical Cells. *Nature* **2001**, *414*, 338−610.

(3) Chen, X.; Mao, S. S. Titanium Dioxide Nanomaterials: Synthesis, Properties, Modifications, and Applications. *Chem. Rev.* **2007**, *107*, 2891−2959.

(4) Fujishima, A.; Zhang, X.; Tryk, D. A. TiO_2 Photocatalysis and Related Surface Phenomena. *Surf. Sci. Rep.* **2008**, *63*, 515−582.

(5) Asahi, R.; Morikawa, T.; Ohwaki, T.; Aoki, K.; Taga, Y. Visible-Light Photocatalysis in Nitrogen-Doped Titanium Oxides. *Science* **2001**, *293*, 269−271.

(6) Murdoch, M.; Waterhouse, G. I. N.; Nadeem, M. A.; Metson, J. B.; Keane, M. A.; Howe, R. F.; Llorca, J.; Idriss, H. The Effect of Gold Loading and Particle Size on Photocatalytic Hydrogen Production from Ethanol over Au/TiO_2 Nanoparticles. *Nat. Chem.* **2011**, *3*, 489−492.

(7) Yang, H. G.; Sun, C. H.; Qiao, S. Z.; Zou, J.; Liu, G.; Smith, S. C.; Cheng, H. M.; Lu, G. Q. Anatase TiO_2 Single Crystals with a Large Percentage of Reactive Facets. *Nature* **2008**, *453*, 638−641.

(8) Diebold, U. The Surface Science of Titanium Dioxide. *Surf. Sci. Rep.* **2003**, *48*, 53−229.

(9) Yu, J.; Xiang, Q.; Ran, J.; Mann, S. One-Step Hydrothermal Fabrication and Photocatalytic Activity of Surface-Fluorinated TiO_2 Hollow Microspheres and Tabular Anatase Single Micro-Crystals with High-Energy Facets. *Chem. Eng. Commun.* **2010**, *12*, 872−879.

(10) Xiang, Q.; Lv, K.; Yu, J. Pivotal Role of Fluorine in Enhanced Photocatalytic Activity of Anatase TiO_2 Nanosheets with Dominant (001) Facets for the Photocatalytic Degradation of Acetone in Air. *Appl. Catal., B* **2010**, *96*, 557−564.

(11) Ohno, T.; Akiyoshi, M.; Umebayashi, T.; Asai, K.; Mitsui, T.; Matsumura, M. Preparation of S-Doped TiO_2 Photocatalysts and their Photocatalytic Activities under Visible Light. *Appl. Catal., A* **2004**, *265*, 115−121.

(12) Irie, H.; Watanabe, Y.; Hashimoto, K. Carbon-Doped Anatase TiO_2 Powders as a Visible-Light Sensitive Photocatalyst. *Chem. Lett.* **2003**, *2*, 772−773.

(13) Lu, N.; Quan, X.; Li, J. Y.; Chen, S.; Yu, H. T.; Chen, G. H. Fabrication of Boron-Doped TiO_2 Nanotube Array Electrode and Investigation of its Photoelectrochemical Capability. *J. Phys. Chem. C* **2007**, *111*, 11836−11842.

(14) Yu, J.; Li, Q.; Liu, S.; Jaroniec, M. Ionic-Liquid-Assisted Synthesis of Uniform Fluorinated B/C-Codoped TiO_2 Nanocrystals and Their Enhanced Visible-Light Photocatalytic Activity. *Chem.—Eur. J.* **2013**, *19*, 2433−2441.

(15) Thompson, T. L.; Yates, J. T. Surface Science Studies of the Photoactivation of TiO_2—New Photochemical Processes. *Chem. Rev.* **2006**, *106*, 4428−4453.

(16) Yu, J.; Dai, G.; Xiang, Q.; Jaroniec, M. Fabrication and Enhanced Visible-Light Photocatalytic Activity of Carbon Self-Doped TiO_2 Sheets with Exposed {001} Facets. *J. Mater. Chem.* **2011**, *21*, 1049−1057.

(17) Pan, J.; Liu, G.; Lu, G. Q.; Cheng, H. M. On the True Photoreactivity Order of {001}, {010}, and {101} Facets of Anatase TiO_2 Crystals. *Angew. Chem., Int. Ed.* **2011**, *50*, 2133−2137.

(18) X. Q. Gong, A. S. Reactivity of Anatase TiO_2 Nanoparticles: The Role of the Minority (001) Surface. *J. Phys. Chem. B* **2005**, *109*, 19560−19562.

(19) Wu, B. H.; Guo, C. Y.; Zheng, N. F.; Xie, Z. X.; Stucky, G. D. Nonaqueous Production of Nanostructured Anatase with High-Energy Facets. *J. Am. Chem. Soc.* **2008**, *130*, 17563−17567.

(20) Yang, H. G.; Liu, G.; Qiao, S. Z.; Sun, C. H.; Jin, Y. G.; Smith, S. C.; Zou, J.; Cheng, H. M.; Lu, G. Q. Solvothermal Synthesis and Photoreactivity of Anatase TiO_2 Nanosheets with Dominant {001} Facets. *J. Am. Chem. Soc.* **2009**, *131*, 4078−4083.

(21) Han, X. G.; Kuang, Q.; Jin, M. S.; Xie, Z. X.; Zheng, L. S. Synthesis of Titania Nanosheets with a High Percentage of Exposed (001) Facets and Related Photocatalytic Properties. *J. Am. Chem. Soc.* **2009**, *131*, 3152−3153.

(22) Dai, Y. Q.; Cobley, C. M.; Zeng, J.; Sun, Y. M.; Xia, Y. N. Synthesis of Anatase TiO_2 Nanocrystals with Exposed {001} Facets. *Nano Lett.* **2009**, *9*, 2455−2459.

(23) Liu, G.; Yang, H. G.; Wang, X. W.; Cheng, L. N.; Pan, J.; Lu, G. Q.; Cheng, H. M. Visible Light Responsive Nitrogen Doped Anatase TiO_2 Sheets with Dominant {001} Facets Derived from TiN. *J. Am. Chem. Soc.* **2009**, *131*, 12868−12869.
(24) Liu, S.; Yu, J.; Jaroniec, M. Anatase TiO_2 with Dominant High-Energy {001} Facets: Synthesis, Properties, and Applications. *Chem. Mater.* **2011**, *23*, 4085−4093.
(25) Gordon, T. R.; Cargnello, M.; Paik, T.; Mangolini, F.; Weber, R. T.; Fornasiero, P.; Murray, C. B. Nonaqueous Synthesis of TiO_2 Nanocrystals Using TiF_4 to Engineer Morphology, Oxygen Vacancy Concentration, and Photocatalytic Activity. *J. Am. Chem. Soc.* **2012**, *134*, 6751−6761.
(26) Zhang, H.; Liu, P.; Li, F.; Liu, H.; Wang, Y.; Zhang, S.; Guo, M.; Cheng, H.; Zhao, H. Facile Fabrication of Anatase TiO_2 Microspheres on Solid Substrates and Surface Crystal Facet Transformation from {001} to {101}. *Chem.—Eur. J.* **2011**, *17*, 5949−5957.
(27) Lu, T.; Zhang, R.; Hu, C.; Chen, F.; Duo, S.; Hu, Q. TiO_2−Graphene Composites with Exposed {001} Facets Produced by A One-Pot Solvothermal Approach for High Performance Photocatalyst. *Phys. Chem. Chem. Phys.* **2013**, *15*, 12963−12970.
(28) Hu, C.; Lu, T.; Chen, F.; Zhang, R.; Lian, C.; Zheng, S.; Hu, Q.; Duo, S. Enhancement of Photocatalytic Performance of TiO_2 Produced by An Alcohothermal Approach through Inclusion of Water. *Mater. Res. Bull.* **2014**, *53*, 42−48.
(29) Zhu, S.; Liang, S.; Gu, Q.; Xie, L.; Wang, J.; Ding, Z.; Liu, P. Effect of Au Supported TiO_2 with Dominant Exposed {001} Facets on the Visible-Light Photocatalytic Activity. *Appl. Catal., B* **2012**, *119*−*120*, 146−155.
(30) Zhang, J.; Xi, J.; Ji, Z. Mo + N Codoped TiO_2 Sheets with Dominant {001} Facets for Enhancing Visible-Light Photocatalytic Activity. *J. Mater. Chem.* **2012**, *22*, 17700−17708.
(31) Li, H.; Zeng, Y.; Huang, T.; Piao, L.; Yan, Z.; Liu, M. Hierarchical TiO_2 Nanospheres with Dominant {001} Facets: Facile Synthesis, Growth Mechanism, and Photocatalytic Activity. *Chem.—Eur. J.* **2012**, *18*, 7525−7532.
(32) Pan, L.; Zou, J. J.; Wang, S.; Liu, X. Y.; Zhang, X.; Wang, L. Morphology Evolution of TiO_2 Facets and Vital Influences on Photocatalytic Activity. *ACS Appl. Mater. Interfaces* **2012**, *4*, 1650−1655.
(33) Lv, K.; Xiang, Q.; Yu, J. Effect of Calcination Temperature on Morphology and Photocatalytic Activity of Anatase TiO_2 Nanosheets with Exposed {001} Facets. *Appl. Catal., B* **2011**, *104*, 275−281.
(34) Xiang, Q.; Yu, J.; Jaroniec, M. Nitrogen and Sulfur Co-Doped TiO_2 Nanosheets with Exposed {001} Facets: Synthesis, Characterization and Visible-Light Photocatalytic Activity. *Phys. Chem. Chem. Phys.* **2011**, *13*, 4853−4861.
(35) Xiang, Q.; Yu, J.; Wang, W.; Jaroniec, M. Nitrogen Self-Doped Nanosized TiO_2 Sheets with Exposed {001} Facets for Enhanced Visible-Light Photocatalytic Activity. *Chem. Commun.* **2011**, *47*, 6906−6908.
(36) Liu, S.; Yu, J.; Jaroniec, M. Tunable Photocatalytic Selectivity of Hollow TiO_2 Microspheres Composed of Anatase Polyhedra with Exposed {001} Facets. *J. Am. Chem. Soc.* **2010**, *132*, 11914−11916.
(37) Chen, H.-S.; Lin, H.-C.; Su, C.; Shen, M.-T.; Li, W.-R. Novel Quasi-Cube TiO_2 Nanoparticles as Light-Scattering Layers for Dye-Sensitized Solar Cells. *J. Nanopart. Res.* **2013**, *15*, 1836−1842.
(38) Huang, Z.; Wang, Z.; Lv, K.; Zheng, Y.; Deng, K. Transformation of $TiOF_2$ Cube to a Hollow Nanobox Assembly from Anatase TiO_2 Nanosheets with Exposed {001} Facets Via Solvothermal Strategy. *ACS Appl. Mater. Interfaces* **2013**, *5*, 8663−8669.
(39) Shuang, Y.; Hou, Y.; Zhang, B.; Yang, H. G. Impurity-Free Synthesis of Cube-Like Single-Crystal Anatase TiO_2 for High Performance Dye-Sensitized Solar Cell. *Ind. Eng. Chem. Res.* **2013**, *52*, 4098−4102.
(40) Wang, B.; Guo, L.; He, M.; He, T. Green Synthesis of TiO_2 Nanocrystals with Improved Photocatalytic Activity by Ionic-Liquid Assisted Hydrothermal Method. *Phys. Chem. Chem. Phys.* **2013**, *15*, 9891−8998.
(41) Antonietti, M.; Kuang, D.; Smarsly, B.; Zhou, Y. Ionic Liquids for the Convenient Synthesis of Functional Nanoparticles and Other Inorganic Nanostructures. *Angew. Chem., Int. Ed.* **2004**, *43*, 4988−4992.
(42) Zhu, Y.-J.; Wang, W.-W.; Qi, R.-J.; Hu, X.-L. Microwave-Assisted Synthesis of Single-Crystalline Tellurium Nanorods and Nanowires in Ionic Liquids. *Angew. Chem., Int. Ed.* **2004**, *43*, 1410−1414.
(43) Zhou, Y.; Antonietti, M. Preparation of Highly Ordered Monolithic Super-Microporous Lamellar Silica with a Room-Temperature Ionic Liquid as Template via the Nanocasting Technique. *Adv. Mater.* **2003**, *15*, 1452−1455.
(44) Dupont, J.; Fonseca, G. S.; Umpierre, A. P.; Fichtner, P. F. P.; Teixeira, S. R. Transition-Metal Nanoparticles in Imidazolium Ionic Liquids: Recycable Catalysts for Biphasic Hydrogenation Reactions. *J. Am. Chem. Soc.* **2002**, *124*, 4228−4229.
(45) Zhao, X.; Jin, W.; Cai, J.; Ye, J.; Li, Z.; Ma, Y.; Xie, J.; Qi, L. Shape- and Size-Controlled Synthesis of Uniform Anatase TiO_2 Nanocuboids Enclosed by Active {100} and {001} Facets. *Adv. Funct. Mater.* **2011**, *21*, 3554−3563.
(46) Jacob, D. S.; Bitton, L.; Grinblat, J.; Felner, I.; Koltypin, Y.; Gedanken, A. Are Ionic Liquids Really a Boon for the Synthesis of Inorganic Materials? A General Method for the Fabrication of Nanosized Metal Fluorides. *Chem. Mater.* **2006**, *18*, 3162−3168.
(47) Li, C.; Gu, L.; Tsukimoto, S.; van Aken, P. A.; Maier, J. Low-Temperature Ionic-Liquid-Based Synthesis of Nanostructured Iron-Based Fluoride Cathodes for Lithium Batteries. *Adv. Mater.* **2010**, *22*, 3650−3654.
(48) Liao, Y.; Zhang, H.; Que, W.; Zhong, P.; Bai, F.; Zhong, Z.; Wen, Qi.; Chen, W. Activating the Single-Crystal TiO_2 Nanoparticle Film with Exposed {001} Facets. *ACS Appl. Mater. Interfaces* **2013**, *5*, 6463−6466.
(49) Liu, B.; Wang, Q.; Yu, S.; Zhao, T.; Han, J.; Jing, P.; Hu, W.; Liu, L.; Zhang, J.; Sun, L.-D.; Yan, C.-H. Double Shelled Hollow Nanospheres with Dual Noble Metal Nanoparticle Encapsulation for Enhanced Catalytic Application. *Nanoscale* **2013**, *5*, 9747−9757.
(50) Hu, W.; Liu, B.; Wang, Q.; Liu, Y.; Liu, Y.; Jing, P.; Yu, S.; Liu, L.; Zhang, J. A Magnetic Double-Shell Microsphere as a Highly Efficient Reusable Catalyst for Catalytic Applications. *Chem. Commun.* **2013**, *49*, 7596−7598.
(51) Li, D.; Haneda, H.; Hishita, S.; Ohashi, N. Visible-Light-Driven N−F-Codoped TiO_2 Photocatalysts. 1. Synthesis by Spray Pyrolysis and Surface Characterization. *Chem. Mater.* **2005**, *17*, 2588−2595.
(52) Wang, J.; Bian, Z.; Zhu, J.; Li, H. Ordered Mesoporous TiO_2 with Exposed (001) Facets and Enhanced Activity in Photocatalytic Selective Oxidation of Alcohols. *J. Mater. Chem. A* **2013**, *1*, 1296−1302.
(53) Sing, K. S. W.; Everett, D. H.; Haul, R. A. W.; Moscou, L.; Pierotti, R. A.; Rouquerol, J.; Siemieniewska, T. Reporting Physisorption Data for Gas/Solid Systems with Special Reference to the Determination of Surface Area and Porosity. *Pure. Appl. Chem.* **1985**, *57*, 603−619.
(54) Wang, W.; Lu, C.; Ni, Y.; Xu, Z. Crystal Facet Growth Behavior and Thermal Stability of {001} Faceted Anatase TiO_2: Mechanistic Role of Gasous HF and Visible-Light Photocatalytic Activity. *CrystEngComm* **2013**, *15*, 2537−2543.
(55) Emeline, A. V.; Kuznetsov, V. N.; Rybchuk, V. K.; Serpone, N. Visible-Light-Active Titania Photocatalysts: The Case of N-Doped TiO_2s—Properties and Some Fundamental Issues. *Int. J. Photoenergy* **2008**, *2008*, 1−19.
(56) Spadavecchia, F.; Cappelletti, G.; Ardizzone, S.; Bianchi, C. L.; Cappelli, S.; Oliva, C.; Scardi, P.; Leoni, M.; Fermo, P. Solar Photoactivity of Nano-N−TiO_2 From Tertiary Amine: Role of Defects and Paramagnetic Species. *Appl. Catal., B* **2010**, *96*, 314−322.
(57) Xiang, Q. J.; Yu, J. G.; Cheng, B.; Ong, H. C. Microwave-Hydrothermal Preparation and Visible-Light Photoactivity of Plasmonic Photocatalyst Ag-TiO_2 Nanocomposite Hollow Spheres. *Chem.—Asian J.* **2010**, *5*, 1466−1474.

(58) Yu, J. G.; Dai, G. P.; Huang, B. B. Fabrication and Characterization of Visible-Light-Driven Plasmonic Photocatalyst Ag/AgCl/TiO_2 Nanotube Arrays. *J. Phys. Chem. C* **2009**, *113*, 16394−16401.
(59) Wu, T. X.; Liu, G. M.; Zhao, J. C.; Hidaka, H.; Serpone, N. Photoassisted Degradation of Dye Pollutants. V. Self-photosensitized Oxidative Transformation of Rhodamine B Under Visible Light Irradiation in Aqueous TiO_2 Dispersions. *J. Phys. Chem. B* **1988**, *102*, 5845−5851.